Active Cluster Wake Mixing

Gutknecht, Jonas; Becker, Marcus; Taschner, Emanuel; Stipa, Sebastiano; Allaerts, Dries; Viré, Axelle; Van Wingerden, Jan Willem

DOI
10.1088/1742-6596/2767/9/092052

Publication date
2024

Document Version
Final published version

Published in
Journal of Physics: Conference Series

Active Cluster Wake Mixing

Active Cluster Wake Mixing

Jonas Gutknecht[1], Marcus Becker[1], Emanuel Taschner[1], Sebastiano Stipa[2], Dries Allaerts[3], Axelle Viré[3], Jan-Willem van Wingerden[1]

[1] Delft University of Technology, Delft Center for Systems and Control, Mekelweg 2, 2628 CD Delft, The Netherlands
[2] University of British Columbia, Okanagan Campus, Canada
[3] Delft University of Technology, Wind Energy Section, Kluyverweg 1, 2629 HS Delft, The Netherlands

E-mail: j.gutknecht@tudelft.nl

Abstract. In recent years, the relevance of the interaction between neighboring wind farms has grown steadily. As one farm extracts energy from the wind, a downstream one can systematically experience lower wind speeds which threatens the economic viability of the farm. Significant progress has been made in understanding these farm-farm wake interactions, but we still lack methodologies to mitigate their undesired effects. In this study, we introduce Active Cluster Wake Mixing (ACWM). This novel method aims to accelerate the recovery of the cluster wake using dynamic control actions: By exciting the thrust of the individual turbines depending on their relative location, we generate non-uniform patterns of energy extraction. Phase offsets between the individual excitation signals propagate these regions through the wind farm. This results in large-scale velocity gradients inside the farm, which also affect the flow in the cluster wake region. An in-depth exploration and optimization of ACWM requires significant computational effort. Therefore, we compare three different wind farm modeling approaches in Large Eddy Simulations (LES) that differ in their computational costs regarding their suitability for further exploration of ACWM. For this purpose, we use an unoptimized ACWM scheme with two different excitation frequencies. For the first time ever we successfully show that ACWM manipulates the flow inside the wind farm with favorable effects on the wake velocity. We also demonstrate that the modeling of cluster wakes is challenging and has a significant effect on the potential gain.

1. Introduction

Wind turbines extract energy from the ambient flow, leaving a less energetic wind in its downstream region, the so-called wake. This may result in a reduction of the extracted power by a downstream turbine by up to 40 % [1]. Understanding, modeling, and minimizing the wake effect has attracted a lot of attention from the research community. Engineering models like the Gaussian wake model [2], FLORIS [3], or FLORIDyn [4] allow for efficient wind farm flow optimization. Concepts like wake steering [5] or dynamic induction control [6, 7] are on advanced technical readiness levels and provide opportunities for increasing a wind farm's efficiency.

The fact, that the energy extraction of multiple wind turbines grouped in a wind farm accumulates to generate an orders of magnitude larger wake than those of a single wind turbine, has just recently started to gain attention. Using satellite synthetic aperture radar (SAR) measurements, Schulz-Stellenfleth et al. [8] observed velocity deficits in the downstream region of wind farms that extend up to 100 km and further during stable atmospheric conditions.

The observed cluster wakes induce a significant reduction of the available kinetic energy at downstream wind farms. These so-called farm-farm interactions are of major importance for the economic viability of offshore wind farm projects in a densely populated offshore environment, as for example the North Sea is planned to be within the next decade. Already nowadays investors are forced to correct their predictions, amongst others due to an underestimation of the farm-farm wake effects [9].

Throughout the last few years, significant advances have been made in understanding the interaction mechanisms of wind farms with the atmospheric flow. Stevens and Menevau [10] describe the development of an internal boundary layer within the atmospheric boundary layer (ABL) due to the declaration of the turbines. The internal boundary layer height grows until it reaches the ABL height to form a fully developed wind turbine array boundary layer (WTABL). Then, phenomena like gravity waves [11] and blockage [12] form out and impact the wind farm efficiency. Calaf et al. [13] show that the power extracted by the wind turbines is of the same order as the vertical fluxes of kinetic energy into the WTABL.

Several studies aim at increasing the vertical fluxes of kinetic energy to maximize the power available to a single wind farm. Goit and Meyers [14] use a receding-horizon optimal control framework to optimize the wind farm control scheme and achieve an increase of the energy extraction by 16 %. Munters and Meyers [15, 6] build up on this work by deriving simplified, sinusoidal control signals that lead to an increased farm-wide power generation of about 5 %. A less conventional approach is taken by VerHulst and Meneveau [16] by applying a synthetic forcing in the vertical direction at the turbine locations. This way an increase of the power extraction by 95 % is archived. The authors highlight that this finding is technically unfeasible, however, it underlines the importance of vertical fluxes of kinetic energy into the wind farm.

Whilst the previous studies focus on a power maximization of one wind farm, Stieren and Stevens [17] examine the effect of spacing and layout on the interaction between two wind farms in a neutral ABL with Large Eddy Simulation (LES). They confirm a significant impact of the wake generated by the upstream wind farm on the flow inside and around a downstream wind farm. A staggered wind farm layout leads to higher energy extraction and consequently a more pronounced wake. They find a reduction of the power production of the first row by 33 % for a wind farm spacing of 5 km and 13 % for a spacing of 15 km.

The first study focusing on the reduction of wake effects beyond one wind farm was presented by Foloppe et al. [18]. They optimize the individual yaw angles of turbines in the Belgium cluster with FLORIS and observe gains for each wind farm. However, the spacing of the wind farms in the Belgium cluster is small enough to consider them as one cluster. Hence, from a physical perspective, they optimize turbine-turbine interaction, not farm-farm interaction as considered in the present study.

To the best of the author's knowledge, all the published studies have focused on maximizing the power generation of one single turbine cluster or understanding the mechanisms of farm-farm interactions. In this work, we present a novel wind farm control method called Active Cluster Wake Mixing (ACWM) that aims at accelerating the cluster wake recovery and thereby increasing the power generation of a downstream wind farm. For this purpose, we dynamically excite the thrust of each turbine depending on its location. Thereby we generate farm-wide patterns of increased or decreased energy extraction that propagate through the wind farm. We show, that depending on the excitation frequency, these perturbations are capable of generating coherent structures in the cluster wake, that lead to increased mean velocity in the wake.

Numerous combinations of thrust patterns and excitation dynamics are possible. The determination of an optimal ACWM scheme requires a high number of computationally expensive LES simulations, considering the domain size necessary to resolve a cluster wake and the simulation time needed to resolve sufficient excitation periods. Consequently, an efficient, reliable LES setup is crucial for an in-depth exploration of ACWM.

The main contribution of this paper is twofold: 1) we demonstrate that with ACWM we can positively influence the cluster wake, and 2) we demonstrate that the potential gain strongly depends on the modeling strategy and that several challenges have to be solved before we can conclude on the potential of ACWM.
The remainder of this paper structures as follows: A detailed explanation of the ACWM principle and implementation in multiple LES environments is given in Section 2. Section 3 presents the results in terms of an analysis of the wake flow and the generated power by the actuated wind farm. A conclusion is given in Section 4.

2. Methodology

2.1. The ACWM principle

The inspiration for ACWM emerged from nature-based observations: Under certain flow conditions, counter-rotating vortices are periodically shed in the wake behind a bluff body. This phenomenon is called *von Kármán vortex street* and can not only be observed under small-scale experimental conditions but also on larger scales, like in the stratocumulus-capped wake of mountainous islands. For instance, Horváth et al. [19] analyze the evolution of a von Kármán vortex street in the wake of Guadalupe island on 9th of May 2018. Combining multiple space-borne measurement techniques, they report the typical oscillating wake with a vortex shedding period of $2-4$ hrs and increased fluctuations of the transverse velocity component.
Stevens et al. [10] confirm that large-scale windfarms interact and interfere with the atmospheric boundary layer, forming blockage and wakes comparably to hills or islands. Additionally, Munters & Meyers [6] and Frederik et al. [7] have shown that dynamic control actions at the turbine can generate coherent vortex structures in the turbine wake that remind to the shape of the von-Kármán-vortex-street and accelerate the wake recovery. Combining the previously described aspects leads to the ACWM-inspiring question: Can a wind farm be controlled such, that dynamics comparable to the von Kármán vortex street are triggered in the cluster wake to enhance the wake velocity?
In this explorative study, we try to trigger these structures in the wake by generating non-uniform, unsteady thrust patterns throughout the wind farm. Each turbine behaves like an individual member of a swarm: Depending on its position, it adapts its thrust to generate farm-wide patterns of increased and decreased energy extraction. A phase shift between the turbine signals allows these patterns to propagate through the wind farm. The spatially non-uniform and unsteady energy extraction results in variations of the wind speed inside the wind farm. In other words, the mean flow is superimposed by a periodic perturbation, that depending on the frequency may grow when propagating into the wake to affect the wake shape and recovery.

2.2. Realization in simulation environment

The previously described ACWM principle includes an unlimited variety of patterns, each with numerous dynamic specifications. We limit this study to one single pattern presented in Figure 1, which we assume to trigger oscillating crosswind motions.
The left panel of Figure 1 visualizes the thrust pattern at the time instance $t = 0$ for a fictitious finite test wind farm with 120 turbines NREL 5 MW [20] in a staggered layout. A spacing of $5D$ in downstream and $4D$ in crosswind direction results in a wind farm length of $l_{x,wf} = 10.08$ km and a wind farm width of $l_{y,wf} = 3.654$ km.
Each dot represents one turbine at its position in the wind farm, colored by the current thrust excitation $C'_{T,e}(t=0)/\hat{C}'_{T,e}$. It is apparent, that the turbines on one half of one row ($y > 0$) increase the thrust, whilst the turbines on the other half of the row ($y < 0$) decrease the thrust. The outermost turbines of each row experience the highest or respectively lowest excitation amplitudes. The excitation amplitudes of the turbines in between are interpolated linearly

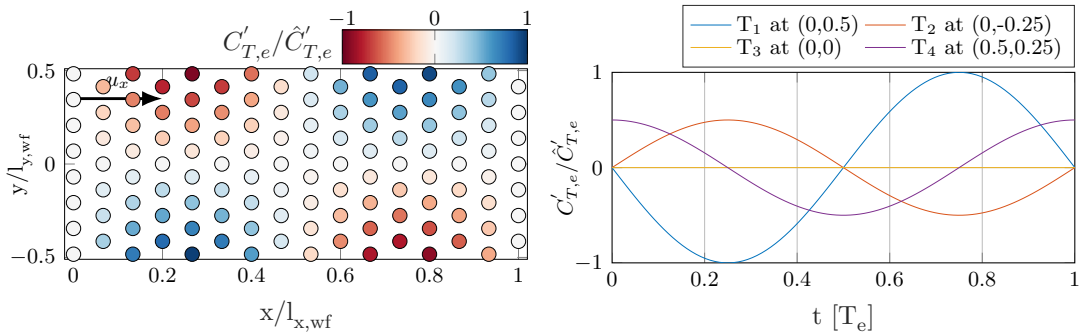

Figure 1. *Left*: Thrust excitation pattern at t=0. Each dot represents one turbine. *Right*: Time series of the thrust excitation for four exemplary turbines T_i at $(x_i/l_{x,wf}\,,\, y_i/l_{y,wf})$.

between those extreme values. The thrust of the turbines in the same row oscillates in phase with an amplitude corresponding to the crosswind position y. The excitation frequency is defined by the Strouhal number St, determined from the wind farm width $l_{y,wf}$ as characteristic length scale, the excitation frequency f_e and the free wind speed u_{inf}:

$$St = \frac{f_e \;\cdot\; l_{y,wf}}{u_{\mathrm{inf}}}. \tag{1}$$

The regions of increased and decreased thrust propagate along the streamwise extension of the wind farm, by phase shifting the excitation signals between the rows. The patterns propagate with a propagation velocity $u_{prop} = 0.7\,u_{\mathrm{inf}}$, such that a volume of air experiences a constant thrust on its way through the wind farm. We thereby aim to enhance the formation of regions with higher and lower wind speed to maximize the effect of ACWM. The described thrust excitation pattern $C'_{T,e}(x,y,t)$ can be parameterized as

$$C'_{T,e}(x,y,t) = \frac{2\cdot\hat{C}'_{T,e}}{l_{y,wf}} \cdot y \cdot \sin\left(2\pi t \;\cdot\; \frac{St\cdot u_{\mathrm{inf}}}{l_{y,wf}} - \frac{\mathrm{mod}(x,\lambda)}{\lambda} 2\pi\right), \quad \lambda = \frac{l_{y,wf}\cdot u_{prop}}{\mathrm{St}\cdot u_{\mathrm{inf}}}, \tag{2}$$

where x represents the downstream position, $\hat{C}'_{T,e}$ the excitation amplitude, t the time and λ the wavelength in downstream direction. Similar to Munters and Meyers [6] we use C'_T which is the thrust coefficient obtained from the effective wind speed at the rotor u_1 instead of C_T obtained from the free wind speed u_{inf}. These thrust excitation patterns are then superimposed with the constant greedy thrust $C'_{T,greedy}$ to obtain the actual thrust distribution throughout the wind farm as $C'_T(x,y,t) = C'_{T,greedy} + C'_{T,e}(x,y,t)$.

The right panel of Figure 1 depicts the excitation time signals of four exemplary turbines T_i at different locations in the wind farm. T_1 and T_2 are located in the same row, hence they oscillate in phase, but due to their different crosswind location, they differ in their amplitudes. T_1 is located at the boundary of the wind farm, hence it reaches $\hat{C}'_{T,e}$. In contrast, T_2 is located at $y = -0.25\,l_{y,wf}$, hence it only reaches half of $\hat{C}'_{T,e}$. The same holds for T_4, which is located at the same distance from the farm center line, but further downstream in the wind farm. Hence the excitation signal is phase-shifted compared to T_1 and T_2. T_3 is located on the wind farm center line, so its thrust does not change.

The exploration of ACWM in terms of flow simulations, including different thrust patterns and excitation frequencies, is related to a high computational effort. This is mostly due to the large domain size needed to capture the cluster wake and the low actuation frequencies that require a

	abbrev.	St	infl.	model
1	BL,AF,L	0	lam	AFM
2	St04,AF,L	0.4	lam	AFM
3	St10,AF,L	1.0	lam	AFM
4	BL,AD,L	0	lam	ADM
5	St04,AD,L	0.4	lam	ADM
6	St10,AD,L	1.0	lam	ADM
7	BL,AD,T	0	PBL	ADM
8	St04,AD,T	0.4	PBL	ADM
9	St10,AD,T	1.0	PBL	ADM

Table 1. Overview cases

grid	1	2	3
x_{lo} [km]	(-5, -9, 0)	(-5, -9, 0)	(-5, -9, 0)
x_{hi} [km]	(35, 9, 1)	(35, 9, 1)	(35, 9, 1)
dx [m]	50x50x10	50x50x20	30x30x10
$x_{ref,lo}$ [km]	-	(-0.5, -3.5, 0)	(-5, -3.5, 0)
$x_{ref,hi}$ [km]	-	(32, 3.5, 0.3)	(35, 3.5, 1)
dx_{ref} [m]	-	30x12.5x10	30x12.5x10
n_{cells} [-]	$29{\cdot}10^6$	$67{\cdot}10^6$	$125{\cdot}10^6$
$t_{wallclock}$ [h]	≈ 12	≈ 24	≈ 48
cases	1,2,3	4,5,6	7,8,9

Table 2. Grid specifications, *ref* denotes the refined grid

long simulation time. Therefore, this study aims on validating the suitability of different wind farm modeling approaches in different inflow conditions, each of them related to an individual computational effort, for an in-depth exploration of ACWM.

2.3. Large Eddy Simulation Setups

We perform Large Eddy Simulations (LES) using the finite-volume LES environment TOSCA (Toolbox fOr Stratified Convective Atmospheres) [21]. TOSCA is a highly parallel efficient tool, tailored to model flows around finite wind farms operating in realistic atmospheric conditions, including gravity-wave interaction with the wind farm, blockage, and farm-farm wake interactions. Its open-source character allows for an adaption of the source code to supply each turbine i with an individual $C'_{T,i}(t)$ time series for implementing the ACWM schemes.
Besides a conventional Actuator Disc Model (ADM) [22] which is validated against ALM simulations in [21], TOSCA also features an Actuator Farm Model (AFM), which can be considered as a canopy model [23] and allows to model each turbine individually, instead of applying a uniform distribution of thrust coefficient per unit area. Due to its reduced complexity and its low grid resolution requirements the AFM requires significantly lower computational effort than ADM simulations. As a result, it represents a promising model candidate for exploring ACWM patterns, worth validating against ADM simulations in this work, since the used AFM version has not been validated yet.

We investigate ACWM in three different case setups: cases 1-3 use the AFM in laminar inflow, which is unrealistic but may serve to explore the concept in a computationally cheap way. Cases 4-6 use ADM in laminar inflow, and cases 7-9 use the ADM in a pressure-driven boundary layer (PBL), see Table 1. According to Goit and Meyers [14] such a PBL sufficiently approximates the behavior of a full conventionally neutral atmospheric boundary layer for turbines situated in the inner layer of the boundary layer. For each of the three setups, we simulate one baseline case in which the turbines are conventionally greedily controlled and two ACWM cases with $St_{0.4} = 0.4$ and $St_{1.0} = 1.0$. For the given wind farm layout and inflow conditions, this corresponds to excitation periods of $T_{e,0.4} = 1015$ s and $T_{e,1.0} = 406$ s. Each case simulates $t_{sim} = 10075$ s. The simulation domain extents for each setup $40 \times 18 \times 1$ km, however the spatial discretization differs. Table 2 summarizes the grid specifications of each setup, where x_{lo} and x_{hi} define two diagonal corners of the grid and dx the spatial discretization in x-,y- and z-direction. The center of the first wind farm row is located at $(0, 0, 0)$. The subscript *ref* refers to the refined grid areas, where the turbines are resolved with 10 grid points in spanwise direction and 12.6 grid points in vertical direction. According to Wu and Porté Agel [24] already five points in spanwise-, and seven points in vertical direction would be sufficient for accurate results with little resolution dependence. For better numerical stability, the cells around the refinement area are shrunk or respectively stretched with factor 0.9 for a smooth transition from fine to coarse grid. The

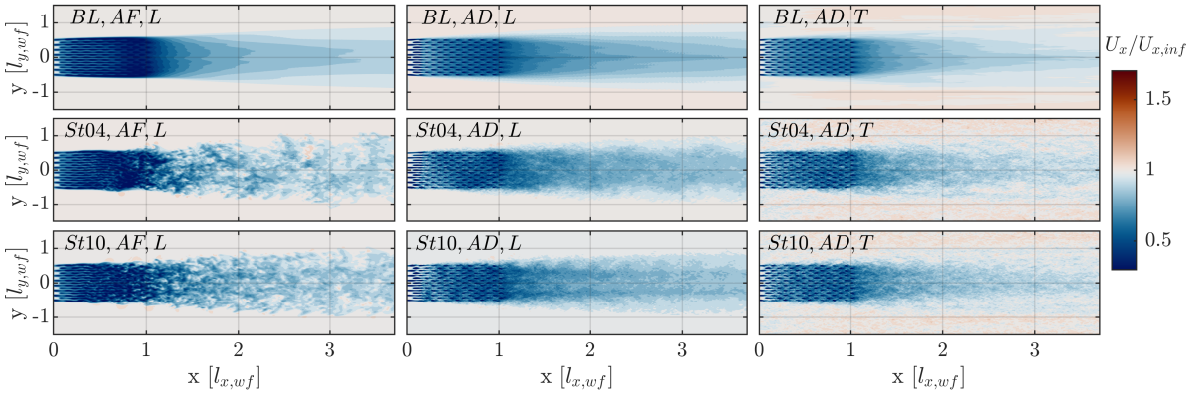

Figure 2. Phase-averaged flow fields for ACWM cases, time-averaged flow fields for baseline cases at hub height, normalized with $U_{x,inf}$.

number of cells increases by approximately factor two between the three grids, which results in the simulation time specified by $t_{wallclock}$ in Table 2 using 600 CPUs on the high-performance cluster *DelftBlue* [25].
The LES code TOSCA uses an adaptive time-stepping scheme, which guarantees the accuracy of the numerical scheme by keeping the Courant-Friederichs-Lewy number $CFL < 0.9$. For the laminar inflow cases, the ground and top surface are modeled as slip walls, the side walls are periodic boundary conditions and the inflow wall is initialized with a constant wind speed of $U_{x,inf} = 9\,\mathrm{ms}^{-1}$. The outlet wall is modeled as zero-gradient boundary condition. For the PBL cases, the ground is modeled as a wall with roughness height $z_0 = 0.001$ using classic Monin Obukhov similarity theory. This results in a precursor with $U_{x,inf,hh} \approx 9\,\mathrm{ms}^{-1}$ at hub height and a turbulence intensity of $TI_{hh} \approx 7\,\%$.

3. Results

This section compares the three LES setups presented in Section 2.3 for their suitability for an in-depth exploration of ACWM. For this purpose we first analyse the phase-averaged flow fields, followed by an investigation of the time-averaged flow quantities. The section closes by comparing the effect on the generated power by the actuated wind farm.

3.1. Phase-averaged Flowfields

The effect of ACWM on the wake shape and the influence of the different model approaches are investigated in terms of the flow fields at hub height. The expected ACWM-generated periodic structures might be superimposed by stochastic fluctuations. Hence we phase-average over the last six simulated periods to filter out these stochastic fluctuations and obtain the periodic structures that match with the excitation frequency. Figure 2 depicts the phase-averaged flow fields of the ACWM cases in the middle and bottom rows. Since the baseline cases do not feature the characteristic periodicity induced by ACWM, the baseline flowfields in the top row are time-averaged over five excitation periods of the $St = 0.4$ ACWM cases $T_{e,0.4}$. Each column presents the results obtained with one LES setup as described in Table 2.

First focusing on the time-averaged baseline flow fields in the top row, Figure 2 reveals a high influence of the simulation setup. These differences affect the flow inside the wind farm at $0 < x < 1\,l_{x,wf}$ as well as for the wake area at $x > 1\,l_{x,wf}$. In the BL, AF, L case, the flow experiences a significantly higher deceleration inside the wind farm, than in the two ADM

cases. This observation was to be expected, as the coarse grid requires larger perturbations to overcome the subgrid model and destabilize the wake. In the turbulent BL, AD, T case the wake appears to recover faster than the two laminar cases. This effect is expected, as the turbulent perturbations are known to contribute to the wake mixing. These characteristics of the different setups need to be kept in mind when discussing the effect of ACWM.

For the ACWM cases in the middle and bottom row of Figure 2 we observe that the flow inside the wind farm is significantly affected by the ACWM thrust patterns. The symmetry along the wind farm center observable in the baseline cases, is no longer present. Instead, regions of faster and slower wind speeds, that alternate in both downstream and crosswind directions can be identified. Size and position of these patterns match to the excitation frequencies. The longer excitation period of the $St = 0.4$ case generates larger regions that are spaced further apart, whereas in the faster oscillating $St = 1.0$ case these regions are smaller and closer to each other. Comparing these regions between the three setups, they differ in terms of their flow deceleration. Due to the more stable wakes in the AFM cases resulting from the coarser grid resolution, they are more pronounced than in the ADM cases, whilst the turbulent mixing in the PBL cases decreases the difference between high- and low-speed regions. However, they can be identified in all the setups, which implies, that even in turbulent conditions, the flow inside the wind farm reacts to the spatially nonuniform energy extraction imposed by the ACWM thrust patterns.

The modification of the internal wind farm flow also affects the flow in the downstream wake region. Comparing the cluster wake within the same setup, its shape differs depending on the control strategy. Especially in the laminar $St = 0.4$ cases, it may be observed that the regions of lower and higher wind speeds propagate beyond the wind farm to generate periodic crosswind deflection in the cluster wake. The periodicity of these deflections scales with the excitation frequency, as their spacing decreases when moving from $St = 0.4$ to $St = 1.0$. In the PBL cases, periodic structures are barely identifiable beyond $x > 2\,l_{x,wf}$, however, also here the wake shape differs depending on the control strategy.

A comparison of the same control strategy throughout the different setups reveals a high sensitivity of the wake to the setup. In the AFM cases, the crosswind deflection of the dominant structures is significantly stronger than in the ADM cases. That deflection reduces significantly when refining the spatial resolution from the laminar AFM cases to the laminar ADM cases. Additionally, the finer resolution leads to less pronounced structures in the wake than in the AFM cases. The accelerated wake recovery in the PBL cases leads to significant deviations from the wake shape observed in the laminar cases.

Conclusively, the phase-averaged flow fields show that ACWM successfully manipulates the shape of the wake. Thereby the excitation frequency governs the periodicity of the generated structures. The intensity of the wake shape manipulation is highly sensitive to the modeling setup. However, none of the investigated cases allows for a quantitative statement concerning the wake recovery.

3.2. Time-averaged Flowfields

Having observed a reaction of the flow to the ACWM schemes in the previous section, this section aims to quantify the effect of ACWM on wake recovery. For this purpose, we analyze the flow fields averaged over five ACWM excitation periods $\bar{U}_x$. The ACWM cases are compared to the baseline cases which are averaged over five excitation periods of the $St = 0.4$ case.

Figure 3 shows the mean hub height velocity averaged over the wind farm width $\bar{U}_{x,wf} = \frac{1}{l_{y,wf}} \int_{-\frac{1}{2}l_{y,wf}}^{\frac{1}{2}l_{y,wf}} \bar{U}_x \, dy$ normalized with the free wind speed $U_{x,inf} = 9\,ms^{-1}$. The laminar AFM cases are plotted in dashed lines, the laminar ADM cases in dotted lines, and the turbulent ADM cases in solid lines. All the cases show a velocity decrease in the wind farm region $0 < x < 1\,l_{x,wf}$, which then recovers in the wake region at $x > 1\,l_{x,wf}$. However, the shapes

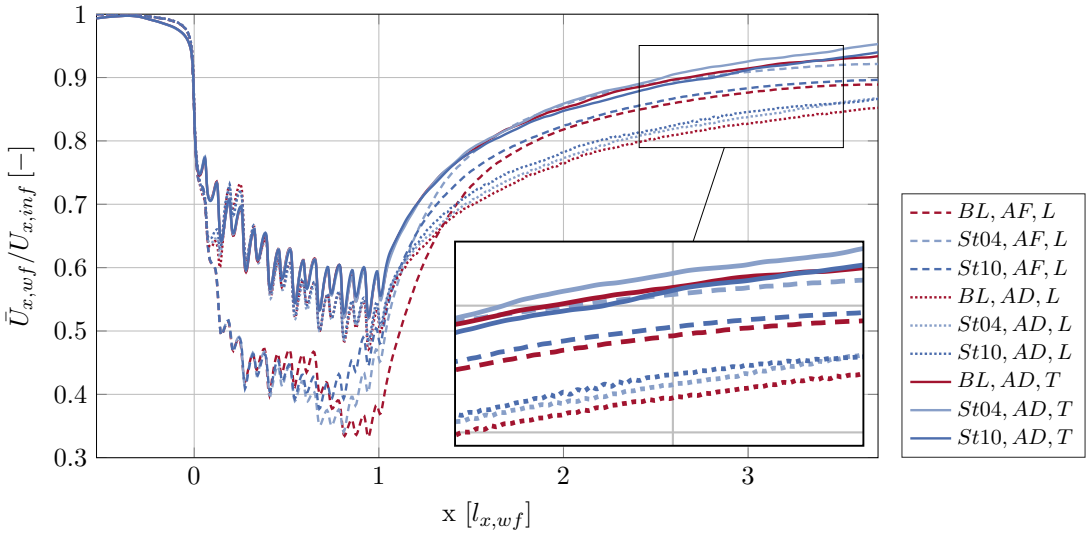

Figure 3. Hub height velocity, averaged over wind farm width and normalized with free wind speed in downstream direction

differ between the setups.
Both laminar and turbulent ADM setups show a velocity drop of about 40 % which matches the power losses found by Porté-Agel et al. [26]. In contrast, the AFM overestimates the losses with about 60 %, which is congruent with the strong flow deceleration observed in the phase averaged flow fields in Figure 2. This observation relates again to the unreasonably stable wakes in laminar inflow on a coarse grid.
Similar to Figure 2, also Figure 3 implies a high sensitivity of the wake to the LES setup. The wakes recover significantly slower in the laminar ADM cases than in the turbulent ADM cases, even though $\bar{U}_{x,wf}$ at the end of the wind farm is approximately equal. The lack of ambient turbulent mixing in the laminar cases explains the slower wake recovery. Notwithstanding the highest velocity deficits at the end of the wind farm, the AFM cases suggest a higher wake velocity than the laminar ADM cases. This is due to the fast diffusion of turbulent structures of a length scale smaller than the grid resolution. On a finer grid, these structures propagate downstream to form a more pronounced wake which is not the case on the coarse grid.
The effect of ACWM is visible in all the setups, however with different intensities. The highest effect may be observed for the AFM cases. Here ACWM already increases the velocity inside the last third of the wind farm. This observation is again due to the coarse grid: without any perturbation in the BL, AF, L case, the wakes of the individual turbines remain stable over a long downstream distance. In contrast in the $St04, AF, L$ and $St10, AF, L$ cases, ACWM induces perturbations that destabilize and accelerate the wake breakdown. Consequently, the mixing with the surrounding flow increases which then results in higher velocities inside the wind farm than in the baseline case. Note, that this effect is not present in the ADM cases. Here, the finer grids resolve smaller turbulent or turbine-induced perturbations which contribute earlier to the wake destabilization. As a result already in the baseline ADM cases the wakes breakdown earlier than in the AFM cases. The additional ACWM perturbations do not affect the turbine wake breakdown, hence the velocity inside the wind farm remains unaffected. Thus it is to conclude, that the flow acceleration toward the end of the wind farm observed in the AFM cases is a numerical artifact that can not be expected in real wind farm flows.

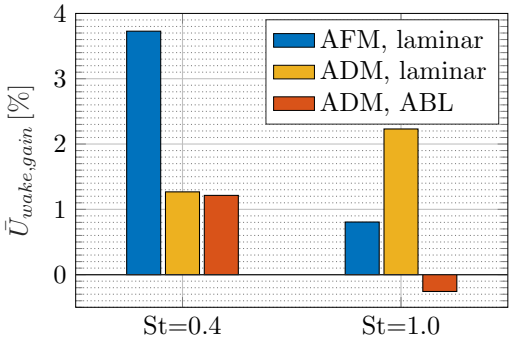

Figure 4. $\bar{U}_{wake,gain}$ at $x = 3\,l_{x,wf}$

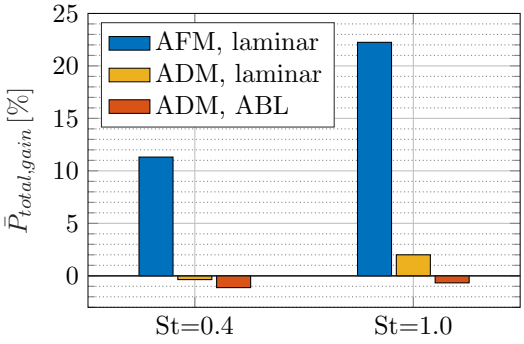

Figure 5. $\bar{P}_{total,gain}$ of actuated wind farm

The effect of ACWM on the cluster wake is particularly strong in the laminar cases. In the AFM as well as the ADM setup, all the ACWM cases show an increased wake velocity throughout the entire wake region. However, the magnitude of the velocity increase depends on the excitation Strouhal number: in the AFM setup $St = 0.4$ generates the highest velocity gains, but in the ADM setup $St = 1.0$ appears to be more efficient. In the PBL setup only $St = 0.4$ leads to velocity gains in the wake, which occur beyond $x \geq 2.5\,l_{x,wf}$. These observations are summarized in Figure 4 in terms of the wake velocity gains $\bar{U}_{wake,gain} = (\bar{U}_{x,wf,ACWM} - \bar{U}_{x,wf,Bl})/\bar{U}_{x,wf,Bl}$ at a downstream position of $x = 3\,l_{x,wf}$. It highlights the trend reversal within the laminar cases: in the AFM setup, $St = 0.4$ performs significantly better than $St = 1.0$, in the ADM setup the opposite is the case. In the PBL setup, which represents the most realistic of the simulated cases, $St = 0.4$ performs the best leading to a wake velocity gain of $\bar{U}_{wake,gain} = 1.2\,\%$. $St = 1.0$, however leads to losses of $\bar{U}_{wake,gain} = -0.26\,\%$.
The analysis of the time-averaged flow proves the capability of ACWM to decrease the velocity deficit in the cluster wake. This holds for computationally cheaper laminar flow conditions, as well as in computationally expensive but more realistic turbulent conditions. However, it also shows that trends, like the dependency of the Strouhal number, highly depend on the case setup and can not be transferred in between the setups.

3.3. Generated Power

Figure 5 depicts the power gains $\bar{P}_{total,gain} = (\bar{P}_{total,ACWM} - \bar{P}_{total,Bl})/\bar{P}_{total,Bl}$ generated by the actuated wind farm. $\bar{P}_{total}$ represents the total power output of the actuated wind farm, averaged over 7560 s. Figure 5 implies an effect of ACWM on the generated power of the actuated wind farm with a high sensitivity to the LES setup. In the laminar AFM cases, ACWM generates power gains of up to 22 %, which are due to the velocity increase at the end of the wind farm observable in Figure 3. As discussed in section 3.2, these velocity gains are a numerical artifact due to the coarse grid, hence, also these power gains can not be assumed realistic.
In the laminar ADM cases, the power gains decrease to $\bar{P}_{total,gain} = -0.36\,\%$ and $\bar{P}_{total,gain} = 2\,\%$ in the $St = 0.4$ and the $St = 1.0$ case, respectively. In a PBL the gains vanish completely and leave power losses of $\bar{P}_{total,gain} \leq -1.12\,\%$.
These observations enforce the implications on the influence of the numerical setup derived previously from the wake analysis: the effect on the generated power is highly sensitive to the setup and a transfer of trends throughout the setups is invalid. Nevertheless, even in the PBL cases, ACWM does not lead to major power losses, even though the investigated excitation schemes are chosen rather randomly for a first tool-chain validation. Further optimization of the ACWM scheme might favorably affect the impact on the generated power.

4. Conclusions

In this study, we introduced Active Cluster Wake Mixing (ACWM), which generates regions of increased and decreased power extraction throughout the farm by exciting the thrust of the individual turbines depending on their location. We successfully showed that the flow inside and behind the wind farm reacts to the nonuniform, unsteady power extraction with potentially favorable effects on the cluster wake velocity and minor effects on the generated power by the actuated wind farm. The efficiency of ACWM was found to be governed by the excitation strouhal number.

These effects of ACWM are achieved with a first unoptimized control scheme. Consequently, we see the potential of optimizing the thrust patterns and actuation frequencies towards higher wake velocity gains and smaller power losses at the actuated wind farm. We investigated three LES setups of different computational costs regarding their suitability for an in-depth exploration of the ACWM idea. Even though the effect of ACWM on the cluster wake can be observed in each of them, we observed a high sensitivity to the LES setup. Trends can not be transferred between the setups, consequently, further exploration of ACWM requires the use of the computationally most expensive PBL setup to prevent misleading conclusions due to modeling errors.

Future work may focus on understanding the effects of ACWM on the interaction between wind farm and the ABL, in particular, its influence on vertical fluxes of mean kinetic energy. These insights may pave the way for an optimal ACWM scheme regarding the effect on wake recovery and power gains.

References

[1] Barthelmie R, Pryor S, Frandsen S, Hansen K S, Schepers J, Rados K, Schlez W, Neubert A, Jensen L and Neckelmann S 2010 *Journal of Atmospheric and Oceanic Technology* **27** 1302–1317
[2] Bastankhah M and Porté-Agel F 2014 *Renewable Energy* **70** 116–123
[3] Gebraad P, Teeuwisse F, Wingerden J W, Fleming P, Ruben S, Marden J and Pao L 2014 *Proceedings of the American Control Conference* 3128–3134
[4] Becker M, Allaerts D and van Wingerden J W 2022 *Journal of Physics: Conference Series* **2265** 032103
[5] Fleming P, Annoni J, Shah J J, Wang L, Ananthan S, Zhang Z, Hutchings K, Wang P, Chen W and Chen L 2017 *Wind Energy Science* **2** 229–239
[6] Munters W and Meyers J 2017 *Philosophical Transactions of the Royal Society A: Mathematical, Physical and Engineering Sciences* **375** 20160100
[7] Frederik J A, Doekemeijer B M, Mulders S P and Wingerden J 2020 *Wind Energy* **23** 1739–1751
[8] Schulz-Stellenfleth J and Djath B 2022 *Handbook of Wind Energy Aerodynamics* 1145–1177
[9] Barlebo M and Andersen A B 2019 Cited 23 January 2023 URL `https://orsted.com/en/company-announcement-list/2019/10/1937002`
[10] Stevens R J and Meneveau C 2017 *Annual Review of Fluid Mechanics* **49** 311–339
[11] Allaerts D and Meyers J 2017 *Journal of Fluid Mechanics* **814** 95â130
[12] Strickland J M, Gadde S N and Stevens R J 2022 *Renewable Energy* **197** 50–58
[13] Calaf M, Meneveau C and Meyers J 2010 *Physics of Fluids* **22** 015110
[14] Goit J and Meyers J 2015 *Journal of Fluid Mechanics* **768** 5â50
[15] Munters W and Meyers J 2017 *Philosophical Transactions of the Royal Society A: Mathematical, Physical and Engineering Sciences* **375** 20160100
[16] VerHulst C and Meneveau C 2015 *Energies* **8** 370–386
[17] Stieren A and Stevens R 2022 *Flow* **2**
[18] Foloppe B, Dewitte L and Munters W 2023 *Journal of Physics: Conference Series* **2505** 012055
[19] Horváth Á, Bresky W, Daniels J, Vogelzang J, Stoffelen A, Carr J L, Wu D L, Seethala C, Günther T and Buehler S A 2020 *Journal of Geophysical Research: Atmospheres* **125** e2019JD032121
[20] Jonkman J, Butterfield S, Musial W and Scott G
[21] Stipa S, Ajay A, Allaerts D and Brinkerhoff J 2023 *Wind Energy Science Discussions* **2023** 1–41
[22] Jimenez A, Crespo A, Migoya E and Garcia J 2007 *Journal of Physics: Conference Series* **75** 012041
[23] Lanzilao L and Meyers J 2023 *Boundary-Layer Meteorology* **186** 1573–1472
[24] Wu Y T and Porté-Agel F 2012 *Boundary-Layer Meteorology* **146**
[25] Delft High Performance Computing Centre (DHPC) 2022 *DelftBlue Supercomputer (Phase 1)*
[26] Porté-Agel F, Wu Y T and Chen C H 2013 *Energies* **6** 5297–5313